THE JOURNAL OF BIOLOGICAL CHEMISTRY VOL. 283, NO. 23, pp. 16235–16247, June 6, 2008

SLC41A1 Is a Novel Mammalian Mg^{2+} Carrier*

Received for publication, August 30, 2007, and in revised form, March 24, 2008 Published, JBC Papers in Press, March 25, 2008, DOI 10.1074/jbc.M707276200

Martin Kolisek[‡1,2], Pierre Launay[§1,3], Andreas Beck[¶1], Gerhard Sponder[‖], Nicolas Serafini[§], Marcel Brenkus[‡], Elisabeth Maria Froschauer[‖], Holger Martens[‡], Andrea Fleig[¶4], and Monika Schweigel[5]**

*From the [‡]Institute of Veterinary-Physiology, FU Berlin, Oertzenweg 19b, D-14163 Berlin, Germany, the [§]INSERM, U699, Equipe Avenir, Paris F-75018, France, the [¶]Laboratory of Cell and Molecular Signalling, Center for Biomedical Research at The Queen's Medical Center, Honolulu, Hawaii 96813, the [‖]Max F. Perutz Laboratories, Department of Microbiology and Genetics, University of Vienna, Dr. Bohrgasse 9, A-1030 Vienna, Austria, and the **Research Institute for the Biology of Farm Animals (FBN), Department of Nutritional Physiology "Oskar Kellner," Wilhelm-Stahl-Alee 2, D-18196 Dummerstorf, Germany*

The molecular biology of mammalian magnesium transporters and their interrelations in cellular magnesium homeostasis are largely unknown. Recently, the mouse SLC41A1 protein was suggested to be a candidate magnesium transporter with channel-like properties when overexpressed in *Xenopus laevis* oocytes. Here, we demonstrate that human SLC41A1 overexpressed in HEK293 cells forms protein complexes and locates to the plasma membrane without, however, giving rise to any detectable magnesium currents during whole cell patch clamp experiments. Nevertheless, in a strain of *Salmonella enterica* exhibiting disruption of all three distinct magnesium transport systems (CorA, MgtA, and MgtB), overexpression of human SLC41A1 functionally substitutes these transporters and restores the growth of the mutant bacteria at magnesium concentrations otherwise non-permissive for growth. Thus, we have identified human SLC41A1 as being a *bona fide* magnesium transporter. Most importantly, overexpressed SLC41A1 provide HEK293 cells with an increased magnesium efflux capacity. With outwardly directed Mg^{2+} gradients, a SLC41A1-dependent reduction of the free intracellular magnesium concentration accompanied by a significant net decrease of the total cellular magnesium concentration could be observed in such cells. SLC41A1 activity is temperature-sensitive but not sensitive to the only known magnesium channel blocker, cobalt(*III*) hexaammine. Taken together, these data functionally identify SLC41A1 as a mammalian carrier mediating magnesium efflux.

Intracellular magnesium, especially its ionized fraction (Mg^{2+}), plays a critical role in enzyme activation, making the ion essential for numerous metabolic processes (1). Mg^{2+} is an important co-factor in a number of other physiological functions, including the synthesis of biomacromolecules, secretion of hormones, and modulation of ion channel activity (2, 3). It is therefore not surprising that an abnormal Mg^{2+} homeostasis is associated with several disease conditions, such as cardiovascular diseases, essential hypertension, diabetes mellitus, and metabolic syndrome (4–6). However, a better understanding of cellular Mg^{2+} transport mechanisms and regulation is needed to elucidate the exact role of Mg^{2+} in these disease processes; at present, this is hampered by limited knowledge of the molecular fundament of the mammalian Mg^{2+} transport network. Despite extensive evidence for the existence of various regulated Mg^{2+} transport proteins (7–10), only two plasma-membrane localized proteins have been identified at the molecular level, namely, TRPM6 and TRPM7, which are ion channels of the melastatin-related transient receptor potential family, and MRS2, a channel located in the inner mitochondrial membrane (11–13). Thus, the recent description of novel putative Mg^{2+} transporters, such as the A1 and A2 members of the solute carrier family 41 (SLC41) (14–17), the ancient conserved domain protein subtype 2 (18, 19), a protein termed magnesium transporter 1 (MagT1) (20) and the protein NIPA1 (21), have significantly expanded the field of research into cellular Mg^{2+} transport systems.

The eukaryotic proteins SLC41A2 and SLC41A3, together with the protein SLC41A1, form a novel and unique family among the SLC superfamily, which contains 44 families of proteins involved in the transport of various inorganic and organic solutes (Ref. 22; HUGO data base). *SLC41A1* was first identified and bioinformatically described by Wabakken *et al.* (14). Human *SLC41A1* (*hSLC41A1*) has been mapped to chromosome 1q31–32 and encodes a protein consisting of 513 amino acids with a predicted molecular mass of 56 kDa (14). In humans and mice, the 5-kb long *SLC41A1* transcripts have been found in most tissues (notably in heart, muscle, testis, thyroid gland, and kidney) (14, 15). Homologues of the *hSLC41A1* have also been identified in worms and insects.

A role of SLC41A1 in Mg^{2+} cellular transport suggests itself because of its partial sequence homology to the bacterial Mg^{2+} transporter MgtE (14, 23, 24). Experiments show that feeding mice on a low Mg^{2+} diet causes increased expression of *SLC41A1* in the kidney, colon, and heart (15). Moreover, analysis of published sequences has predicted SLC41A1 to be an integral cell membrane protein possessing 10 transmembrane domains. However, the only direct experimental evidence for SLC41A1 being an Mg^{2+} transporter has been reported by

* This work was supported, in whole or in part, by National Institutes of Health Grant P01GM078195 (to A. F.). This work was also supported by the Free University Berlin and Protina Pharmazeutische GmbH (to M. K.), and Avenir funding (to P. L.). The costs of publication of this article were defrayed in part by the payment of page charges. This article must therefore be hereby marked "*advertisement*" in accordance with 18 U.S.C. Section 1734 solely to indicate this fact.

[1] These authors contributed equally.
[2] To whom correspondence may be addressed. Tel.: 49-30-83862628; Fax: 49-30-83862610; E-mail: martink@zedat.fu-berlin.de.
[3] To whom correspondence may be addressed. E-mail: pierre.launay@bichat.inserm.fr.
[4] To whom correspondence may be addressed. E-mail: afleig@hawaii.edu.
[5] To whom correspondence may be addressed. E-mail: mschweigel@fbn-dummerstorf.de.

Goytain and Quamme (15). By using a two-electrode-voltage clamp (TEV),[6] the authors suggest that heterologous expression of mouse *SLC41A1* (*mSLC41A1*) in *Xenopus laevis* oocytes induces large inward currents carried by Mg^{2+}.

In this study, we have identified SLC41A1 as an eukaryotic Mg^{2+} carrier with the ability to form protein complexes. We show that SLC41A1 mediates a slow temperature-sensitive transport of Mg^{2+} and, importantly, that it is able to substitute genetically distant bacterial Mg^{2+} transporters CorA, MgtA, and MgtB at a functional level in *Salmonella*. Overall, our data suggest that SLC41A1 is an Mg^{2+} carrier playing a significant role in transmembrane Mg^{2+} transport and, by extrapolation, in cellular Mg^{2+} homeostasis.

EXPERIMENTAL PROCEDURES

Salmonella enterica sv. typhimurium

Strains, Plasmids, Growth Media, and Cultivation Conditions

Strain MM1927—DEL485(LeuBCD), mgtB::MudJ; mgtA21::MudJ; corA45::mudJ; zjh1628::Tn10(cam) Cam^R, Kan^R; *pALTER-corA* (Amp^R).

Strain MM281—DEL485(LeuBCD), mgtB::MudJ; mgtA21::MudJ; corA45::mudJ; zjh1628::Tn10(cam) Cam^R, Kan^R (Mg^{2+} dependent strain). Strains MM1927 and MM281 were kindly provided by M. E. Maguire (Case Western Reserve University, Cleveland, OH).

Strain MM281-pUC18-SLC41A1—DEL485(LeuBCD), mgtB::MudJ; mgtA21::MudJ; corA45::mudJ; zjh1628::Tn10(cam) Cam^R, Kan^R; *pUC18-SLC41A1*.

hSLC41A1 was amplified by PCR from the point mutation-corrected plasmid *pGEM-T-hSLC41A1* (the original plasmid was provided by H.-C. Aasheim, Radium Hospital Oslo, Norway) by using specific primers SLC1-1-6xHis-XbaI, 5′-tgcTCTAGAatgCATCACCATCACCATCACtcctctaagccagag-3′, and SLC2-1-HindIII, 5′-cccAAGCTTctagtccccgacatcc-3′, and cloned into plasmid *pUC18*. The *pUC18-hSLC41A1* and *pUC18-*(*empty*) isolated from *Escherichia coli* were transfected into *Salmonella* transmitter strain LT2-LB5010 (str^R, r^-, m^+) (25). If not otherwise stated, hSLC41A1 expression was induced by addition of 0.05 mmol $liter^{-1}$ isopropyl β-D-thiogalactopyranoside (IPTG) to the growth media.

LB medium containing 10 mmol $liter^{-1}$ $MgCl_2$ was used to culture the MM281 strain. The solid and liquid N-minimal media for complementation tests were prepared according to Nelson and Kennedy (26), except that 0.5 mmol $liter^{-1}$ Na_2SO_4 was used instead of 0.5 mmol $liter^{-1}$ K_2SO_4. In addition, the media were supplemented with 0.1% casamino acids (Difco BD) and thiamine (2 mg $liter^{-1}$, Sigma). Overnight cultures grown in LB medium (37 °C, provided with Mg^{2+} if necessary) were washed with 0.7% saline, adjusted to an A_{600} of 0.1 and diluted as indicated in Fig. 4. Serial dilutions were spotted onto N-minimal medium plates containing 10 mmol $liter^{-1}$, 100 μmol $liter^{-1}$, or 10 μmol $liter^{-1}$ $MgCl_2$. Spotted bacteria were cultivated for 36 h. To establish growth curves, overnight cultures grown in LB medium were washed with 0.7% saline, adjusted to an A_{600} of 0.1, and inoculated into liquid N-minimal media containing 10 mmol $liter^{-1}$, 100 μmol $liter^{-1}$, or 10 μmol $liter^{-1}$ $MgCl_2$.

Immunoprecipitation and Western Blot Analysis

Total proteins were extracted from 250 ml of the bacterial culture (−IPTG or +IPTG, as indicated) using trichloroacetic acid/acetone. Proteins of the membrane fraction were isolated using the ProteoExtract™ Partial Bacterial Proteome Extraction Kit (Calbiochem, La Jolla, CA). His-tagged hSLC41A1 was immunoprecipitated from the membrane protein fraction with a His_6 tag antibody (GenWay Biotech, San Diego, CA). Protein samples were separated by SDS-PAGE utilizing 12.5% polyacrylamide gels, blotted, and labeled with His_6 tag antibody and goat anti-mouse (GAM)-HRP (Molecular Probes, Eugene, OR) or GAM-κ-HRP (SBA, Birmingham, AL) antibodies. Antibody binding was visualized using the Chemilmager™ 5500 (Alpha Innotech) or AGFA Cronex 5 medical x-ray films developed with the Curix 60 (AGFA).

Determination of Total Magnesium in Salmonella by ICP-Mass Spectroscopy (ICP-MS)

Cultures of strains MM1927, MM281, and MM281-pUC18-hSLC41A1, grown (24 h) in N-minimal medium supplemented with 2 or 10 mmol $liter^{-1}$ Mg^{2+}, were washed 3 times with 0.7% saline and diluted to a bacterial density of 3×10^8 bacteria ml^{-1}. Diluted bacterial suspensions (1 ml each) were centrifuged. Dried bacterial pellets were resuspended in 0.3 ml of 1 N HNO_3 and 0.7 ml of 1-bromododecane (*purum-purum*, Roth Karlsruhe Germany). Samples were centrifuged and the upper water fractions were used to determine total magnesium content (ICP-MS ELAN 6100, PerkinElmer Life Sciences). The organic fractions were used to determine protein content.

Determination of Free Intracellular Mg^{2+} in Salmonella by mag-fura 2 FF-Spectrofluorometry

Experimental procedures and data analyses were conducted according to Froschauer *et al.* (27) except the mag-fura 2 AM loading facilitator Pluronic F-127 was used at a final concentration of 5 μmol $liter^{-1}$ and the mag-fura 2 AM loading period was 30 min. Measurements were performed with LS-55 spectrofluorometer, operated by FL WinLab software version 4.0 (both products of Perkin-Elmer) at 37 °C, in 3-ml cuvettes containing bacterial suspension (2 ml, 3×10^8 bacteria ml^{-1}).

HEK293- and HEK293-derived Cell Lines

Growth Media and Culture Conditions

HEK293-(FLAG-SLC41A1)—Full-length hSLC41A1 cDNA was cloned into a modified version of the *pCDNA4/TO* vector (Invitrogen) with an N-terminal FLAG tag. The *FLAG-hSLC41A1* cDNA in *pCDNA4/T0* was electroporated into HEK293 cells previously transfected with the *pCDNA6/TR*

[6] The abbreviations used are: TEV, two-electrode-voltage clamp; IPTG, isopropyl β-D-thiogalactopyranoside; HRP, horseradish peroxidase; ICP-MS, ICP-mass spectroscopy; PBS, phosphate-buffered saline; BAPTA, 1,2-bis(2-aminophenxyl)ethane-*N*,*N*,*N*′,*N*′-tetraacetic acid; HBS, Hanks buffered saline; DIDS, 4,4′-diisothiocyanostilbene-2,2′-disulfonic acid; ATPγS, adenosine 5′-*O*-(thiotriphosphate); WT, wild type; CoHex, cobalt(*III*) hexaammine; $[Mg^{2+}]_i$, intracellular $[Mg^{2+}]$; $[Mg]_{t_2}$, total [Mg]; ICP, inductively coupled plasma.

construct for Tet-repressor expression. Cells were placed under zeocin selection; zeocin-resistant clones were screened for tet-inducible expression of the FLAG-tagged hSLC41A1 protein.

Tet-inducible HEK293-(FLAG-SLC41A1) cells were cultured in Dulbecco's modified Eagle's medium (Biochrom AG, Berlin, Germany) containing 10% fetal bovine serum (PAN Biotech, Aidenbach, Germany), 2 mmol liter^{-1} glutamine (PAN Biotech), PenStrep (PAN Biotech), Normocin^{TM} (0.1 mg ml^{-1}, Cayla Toulouse France), blasticidin (5 μg ml^{-1}, Cayla), and zeocin (0.4 mg ml^{-1}, Cayla). *FLAG-SLC41A1* overexpression was induced with tetracycline (1 μg ml^{-1}, Fluka Germany).

HEK293-(HA-TRPM7)—Cultivation conditions were as described in Schmitz *et al.* (12).

HEK293—Cells were cultured in Dulbecco's modified Eagle's medium supplemented with 10% fetal bovine serum, 2 mmol liter^{-1} glutamine, PenStrep, and Normocin.

Immunoprecipitation and Western Blot Analysis

Non-induced (−tet) and induced (+tet, 15–18 h) HEK293-(FLAG-SLC41A1) cells (10^7 cells ml^{-1}) were lysed for 30 min at 4 °C in Tris buffer (pH 7.5) containing 1% Triton X-100 (Bio-Rad) and protease inhibitors. Membrane protein fraction was isolated from the same cell types with ProteoExtract^{TM} Native Membrane Protein Extraction Kit (M-PEK, Calbiochem). Both, total lysate proteins and membrane fraction proteins had been resolved by 10% SDS-PAGE, transferred to polyvinylidene difluoride membranes, and immunodecorated with anti-FLAG antibody coupled to HRP (Invitrogen), or with antibody to β-actin (AbCam, Cambridge, UK) conjugated to GAM HRP-linked antibody (Jackson ImmunoResearch Laboratories, West Grove, PA).

The same samples were immunoprecipitated by M2 anti-FLAG (Sigma) or isotype control, resolved by 10% SDS-PAGE, and transferred to polyvinylidene difluoride membranes. The membrane was immunoblotted with M2 anti-FLAG (Sigma) and GAM-κ-HRP (SBA, Birmingham, AL). Membranes were developed by enhanced chemical luminescence (ECL) (Amersham Biosciences).

Blue-native Polyacrylamide Gel Electrophoretic (BN-PAGE) Separation and Two-dimensional SDS-PAGE

Enriched native membrane proteins were isolated from +tet (15 h) HEK293-(SLC41A1) cells by use of the ProteoExtract^{TM} M-PEK. Native protein samples were mixed with SDS and incubated for 10 min in a thermomixer at 37 °C with moderate shaking before being separated on the BN-polyacrylamide gel gradient (4 > 12%) according to the protocol of Swamy *et al.* (28). Proteins forming complexes with SLC41A1 were resolved by two-dimensional 10% SDS-PAGE and stained with Silver Stain Plus (Bio-Rad). The two-dimensional gels running in parallel with those used for silver staining were blotted and immunodecorated with M2 anti-FLAG and GAM HRP-linked antibodies and FLAG-SLC41A1 was visualized by a Chemilmager^{TM} 5500 (Alpha Innotech). Protein marker Native Mark^{TM} was purchased from Invitrogen.

Confocal Microscopy

5×10^5 HEK293-(FLAG-SLC41A1) cells were plated on 12-mm glass, gelatin (2%)-coated coverslips and cultured for 24 h. Thereafter, FLAG-hSLC-41A1 overexpression was induced with tetracycline (15 h). Then, labeling of +tet and −tet cells with Alexa Fluor-594 wheat germ agglutinin (2 μg ml^{-1}, 10 min at 4 °C) purchased from Invitrogen was performed. After rinsing with phosphate-buffered saline (PBS), cells were fixed in 100% methanol (10 min at −20 °C). All following steps were carried out at room temperature. Cells were rinsed with PBS, blocked for 1 h in PBS containing 0.5% fish skin gelatin (Sigma), and then rinsed with PBS containing 0.02% fish skin gelatin. Subsequently, they were incubated for 45 min each with the primary M2 anti-FLAG antibody (1 mg ml^{-1}) and with the secondary GAM antibody (0.4 mg ml^{-1}, Invitrogen) labeled with Alexa Fluor-488. Processed samples were coated with 5 μl of vectashield (Vector Laboratories, Burlingame, CA) and digital images were acquired using a confocal microscope Zeiss LSM 510 META (Zeiss Jena Germany). Colocalization correlation analysis was performed using the Zeiss LSM 510 Image Browser (Zeiss).

Electrophysiology

Whole cell mode patch clamp experiments were performed at 21–25 °C. Data were acquired with Pulse software controlling an EPC-9 amplifier (HEKA Lambrecht/Pfalz Germany) with settings as described in Schmitz *et al.* (12). Coverslip-grown −tet and +tet HEK293-(SLC41A1) and HEK293-(TRPM7) cells were kept, during all experiments, in a Ringer solution in the following composition (in mmol liter^{-1}): NaCl 140, KCl 2.8, $CaCl_2$ 1, $MgCl_2$ 2, HEPES 10, glucose 10, the pH being adjusted to 7.2 with NaOH. SLC41A1 intracellular pipette-filling buffer contained (in mmol liter^{-1}): K^+-Glu 140, NaCl 8, HEPES 10, the pH being adjusted to 7.2 with NaOH. TRPM7 intracellular pipette-filling buffer contained (in mmol liter^{-1}): Cs^+-Glu 140, NaCl 8, HEPES 10, Cs^+-BAPTA 10, the pH being adjusted to 7.2 with CsOH. In one series of experiments, a low Cl^- Ringer solution (in mmol liter^{-1}: sodium glutamate 140, KCl 2.8, $CaCl_2$ 1, $MgCl_2$ 2, HEPES 10, glucose 10, pH 7.2) was applied externally and the cells were perfused with KCl-based SLC41A1 intracellular pipette-filling buffer (containing in millimole liter^{-1}: KCl 140 instead of K^+-Glu 140). The final osmolarity of each of the above buffers was ~300 mOsm.

Determination of Free Intracellular Mg^{2+} in +tet and −tet HEK293-(SLC41A1) Cells by mag-fura 2 FF-Spectrofluorometry

The −tet and +tet HEK293-(SLC41A1) cells were rinsed twice with ice-cold, completely divalent-free PBS, detached by use of Hytase (Perbio Science, Bonn, Germany), centrifuged, washed twice in PBS, and finally re-suspended in completely Ca^{2+}- and Mg^{2+}-free Hanks balanced solution (CMF-HBS, pH 7.4, PAN Biotech). Loading of cells with 7.5 μmol liter^{-1} mag-fura 2 AM (Molecular Probes) was performed for 25 min at 37 °C in the presence of pluronic acid. After being washed in CMF-HBS, cells were incubated for a further 30 min to allow for complete de-esterification of the fluorescence probe, washed twice in CMF-HBS to remove extracellular mag-fura 2, and

stored in CMF-HBS complemented with 10 mmol liter^{-1} HEPES and 5 mmol liter^{-1} glucose (CMF-HBS+) until used for measurements of free intracellular [Mg^{2+}] ([Mg^{2+}]$_i$). Measurements were made at 37 °C (or as indicated under "Results") in 3-ml cuvettes containing cell suspension (2 ml, CMF-HBS+ with a cytocrit of 10%) under stirring after the cells had been washed twice in CMF-HBS+. In experiments with inside-directed Mg^{2+} gradients, $MgCl_2$ was added to give final concentrations of 2, 5, or 10 mmol liter^{-1} (30 to 40 s prior to start of the measurements). In control measurements, no Mg^{2+} was added but, instead, 2, 5, or 10 mmol liter^{-1} Ca^{2+} was present in the measuring solution. [Mg^{2+}]$_i$ was determined by measuring the fluorescence of the probe-loaded cells in a spectrofluorometer (LS50-B, PerkinElmer Life Sciences) by using the fast filter accessory, which allowed fluorescence to be measured at 20-ms intervals with excitation at 340 and 380 nm, and emission at 515 nm. [Mg^{2+}]$_i$ values were calculated from the 340/380-nm ratio according to the formula of Grynkiewicz *et al.* (29) using FL WinLab version 4.0 (PerkinElmer Life Sciences). A dissociation constant of 1.5 mmol liter^{-1} for the mag-fura 2-Mg^{2+} complex was used for calculations; minimum (R_{min}) and maximum (R_{max}) ratios were determined at the end of each experiment by using digitonin. R_{max} was found by the addition of 25 mmol liter^{-1} $MgCl_2$ in the absence of Ca^{2+}, whereas R_{min} was obtained by addition of 50 mmol liter^{-1} EDTA, pH 7.2, to remove all Mg^{2+} from the solution. For data evaluation, 10-s data sets each were averaged at the beginning of the measurement and then always after 50 s. The final [Mg^{2+}]$_i$ was determined as the mean [Mg^{2+}]$_i$ of the last 10 s of the measurement. Thus, for the calculation of any given [Mg^{2+}]$_i$, 500 data points were used. If not otherwise stated, data are presented as mean ± S.E.

Determination of Free Intracellular Ca^{2+} in +tet and −tet HEK293-(SLC41A1) Cells by fura 2 FF-Spectrofluorometry

The general procedure was the same as that described for the determination of [Mg^{2+}]$_i$ with the following exceptions. Cells were loaded with 10 μmol liter^{-1} fura 2 AM. The R_{max} for fura 2 was obtained in solutions with 2 mM Ca^{2+} and the R_{min} by the addition of 20 mmol liter^{-1} EGTA, pH 8.0; a dissociation constant of 224 nmol liter^{-1} was used for the fura 2-Ca^{2+} complex.

Determination of the Total Mg in −tet and +tet (15 h) HEK293-(FLAG-SLC41A1) by Atomic Mass Spectroscopy

The −tet and +tet (15 h) HEK293-(FLAG-SLC41A1) cells were grown to ~80% confluence, washed twice with serum-free, Mg^{2+}/Ca^{2+}-free HEK293 experimental medium (PAN Biotech), detached by 0.25% trypsin-EDTA buffer, and resuspended in HEK293 medium to give a final cell count of 6×10^6 cells ml^{-1}. The viability of the cells was determined using trypan blue exclusion. Diluted cells were held in the synthetic HEK293 medium for 60 min prior to the addition of Mg^{2+} to give a final [Mg^{2+}]$_e$ of 10 mmol liter^{-1}. Subsequently, the cells were incubated in the presence of Mg^{2+} at 37 °C in 5% CO_2 atmosphere for 20 or 180 min. After incubation, they were washed three times with Mg^{2+}/Ca^{2+}-free PBS and dried pellets were mixed with 0.3 ml of 1 N HNO_3 and 0.7 ml of 1-bromododecane (*purum-purum*). Samples were centrifuged and the upper water fractions were used to determine total magnesium contents (flame AM Spectrometer M Series, Thermo Scientific). Protein contents were determined in the organic fractions.

Statistics

All statistical calculations were performed by using SigmaStat (Jandel Scientific). Significance was determined by Student's *t* test; $p < 0.05$ was considered to be significant.

Inhibitors

DIDS and cobalt(*III*) hexaammine (CoHex) were obtained from Sigma. H_2DIDS was purchased from Molecular Probes.

RESULTS

To assess the basic molecular characteristics of SLC41A1 and its role in cellular Mg^{2+} transport, we took advantage of the well established tetracycline-controlled expression system in the HEK293 cell line. Several zeocin-resistant clones were tested; clone 17 was selected for this study, because of the high level of overexpression and the lack of molecular leakiness (Fig. 1, *B* and *C*).

Cell Topography of Recombinant FLAG-hSLC41A1—Computational analyses predicted SLC41A1 to be an integral cell membrane protein with 10 putative transmembrane domains and possibly both N and C termini located intracellularly (Fig. 1*A*) (14, 15) (PSORT II and WOLF PSORT II Prediction). To test whether overexpressed *FLAG-hSLC41A1* was targeted to the plasma membrane of the HEK293 cells, we designed several experiments comprising confocal immunolocalization and Western blot analysis of the membrane protein fraction isolated from non-induced (−tet) and tet-induced (+tet) HEK293-(FLAG-hSLC41A1).

As shown in Fig. 1*B*, the recombinant FLAG-tagged SLC41A1 protein was specifically detected in the plasma membrane of +tet (15 h) HEK293-(FLAG-hSLC41A1) cells investigated by confocal microscopy. This was confirmed by colocalization of the green fluorescent signal of immunolabeled hSLC41A1 (M2 anti-FLAG: GAM Alexa 488) with the red fluorescent signal of wheat germ agglutinin conjugated to Alexa 594 (Fig. 1*B*). The latter is known to recognize sialic acid and *N*-acetylglucosaminyl sugar residues predominantly found on the plasma membrane. Colocalization correlation analysis revealed a 59.3 ± 1.6% overlap of red and green pixels. In contrast, no FLAG-hSLC41A1-specific fluorescence was found in −tet cells (Fig. 1*B*). Fig. 1*C* shows data obtained by Western blot analysis of membrane protein fractions and non-membrane protein fractions from −tet and +tet (18 h) cells. The 56-kDa band corresponding to FLAG-hSLC41A1 was predominantly detected in the membrane fraction with lower abundance in the non-membrane fraction. Western blot analysis of immunoprecipitated FLAG-hSLC41A1 from membrane and non-membrane protein fraction lysates revealed the same results (Fig. 1*C*). FLAG-hSLC41A1-specific band was not detected in samples prepared from −tet cells. Taken together, these data demonstrate the plasma membrane localization of FLAG-hSLC41A1 when overexpressed in HEK293 cells (Fig. 1*A*).

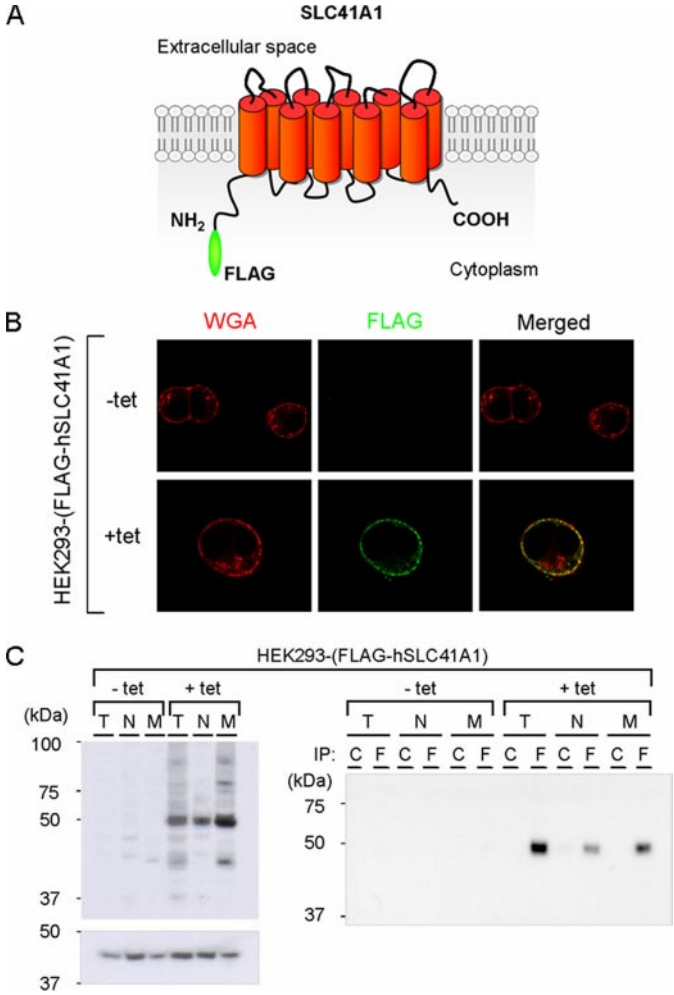

FIGURE 1. **Expression and cellular localization of FLAG-hSLC41A1 (56 kDa) in HEK293-(FLAG-SLC41A1) cells.** *A*, the most probable computer-predicted model of SLC41A1 membrane topology. *B*, confocal immunolocalization of FLAG-hSLC41A1, in −tet and +tet (15 h) cells. FLAG-SLC41A1 immunolabeled with primary M2 anti-FLAG and secondary GAM Alexa 488 antibodies (*green* signal) was detected exclusively in the cytoplasmatic membrane of +tet cells. Plasma membranes of both −tet and +tet cells were fluorescently contrasted with WGA conjugated to Alexa 594 (*red* signal). The *yellow* color in the merged image show that both signals colocalize in +tet cells. *WGA*, wheat germ agglutinin. *C*, immunodetection of recombinant FLAG-hSLC41A1 in total protein isolate (*T*), non-membrane protein fraction (*N*) and membrane protein fraction (*M*) of −tet and +tet (18 h) HEK293-(FLAG-SLC41A1) cells. FLAG-SLC41A1 was immunodetected with anti-FLAG-HRP antibody or M2 anti-FLAG: GAM-κ-HRP antibodies. Reference β-actin bands were immunodetected with anti-β-actin: GAM-HRP antibodies. No FLAG-hSLC41A1 was detected in −tet cells. The highest hSLC41A1 abundance was detected in the M fraction of +tet cells. This was confirmed by Western blot analysis performed with FLAG-hSLC41A1 immunoprecipitated (*IP*) from T, N, and M. In both cases protein samples were resolved by 10% SDS-PAGE; *C*, isotype control; *F*, FLAG tag.

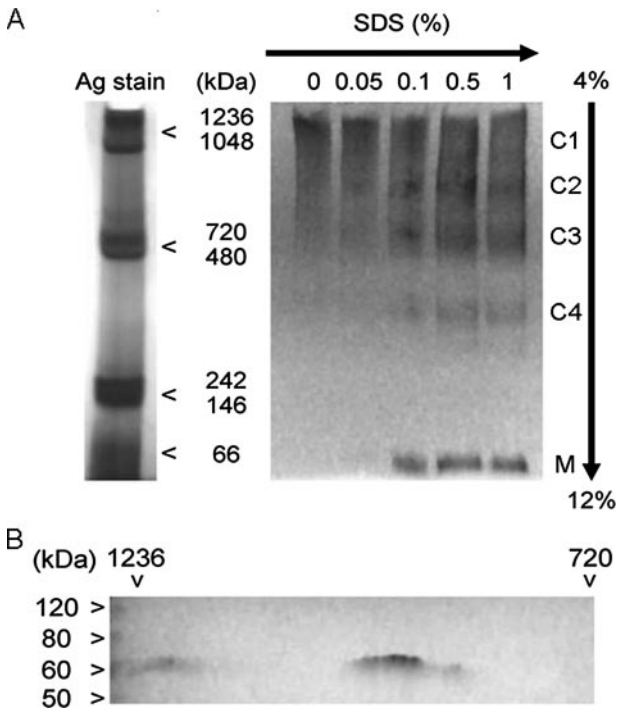

FIGURE 2. **Complex forming ability of hSLC41A1 in HEK293-(FLAG-SLC41A1) cells.** FLAG-SLC41A1 was immunodetected with M2 anti-FLAG: GAM-HRP antibodies. *A*, gradient BN-PAGE (4–12%) analysis of SLC41A1 complexes. Successively increasing SDS concentration (as indicated) lead to break-down of high molecular mass complexes C1 and C2 resulting in appearance of SLC41A1 complexes with "lower" molecular mass (*C3*, *C4*) and of monomeric SLC41A1 (*M*). *B*, presence of SLC41A1 in C1 and C2 complexes verified by two-dimensional SDS-PAGE followed by immunodecoration of SLC41A1.

Complex Forming Ability of hSLC41A1—Various solute transporters have been shown to form stable or transient protein complexes, which are necessary for them to be functional (31, 32). To test whether hSLC41A1 formed such complexes with other proteins, we performed BN-PAGE with native proteins isolated from +tet (15 h) HEK293-(SLC41A1) cells. FLAG-hSLC41A1-containing complexes were immunodetected with M2 anti-FLAG and goat anti-mouse HRP-linked antibodies. We identified two complexes (C1 and C2; Fig. 2*A*) with molecular masses lying between 720 and 1236 kDa (720 kDa < C1, C2 < 1236 kDa). Next, the hSLC41A1 complexes were gradually degraded by adding SDS in a stepwise manner to give concentrations from 0.05 to 1%. Upon addition of 0.1% SDS, we were able to detect the break-down products of C1 and C2: 480 kDa < C3 < 720 kDa; 242 kDa < C4 < 480 kDa and M ~56 kDa, the latter corresponding to the molecular mass of the SLC41A1 monomer (Fig. 2*A*). A successive increase of SDS strengthened the signal of C4 and M and, as expected, weakened the signal of C1 and C2. The two-dimensional SDS-PAGE separation of the C1 and C2 complexes followed by silver staining revealed heterogeneous compositions of C1 and C2 complexes (data not shown). Because of the limited resolution of the high molecular mass protein complexes (750 kDa ≪ Cx) in the first native dimension, the presence of SLC41A1 in C1 and C2 complexes was confirmed by SLC41A1 immunodecoration after two-dimensional SDS-PAGE (Fig. 2*B*).

Effect of hSLC41A1 Overexpression on Growth and Mg^{2+} Content of Mg^{2+}-deficient Salmonella Strain MM281—The *hSLC41A1* gene shares sequence similarity with the bacterial gene mgtE (14, 15). Gene mgtE has been identified in various bacteria (23, 24), but not in *Salmonella sp*. Based on its ability to restore growth of the Mg^{2+}-deficient strain MM281 of *S. enterica,* Smith and colleagues (24) have proposed the direct involvement of MgtE in Mg^{2+} transport. Strain MM281 exhibits disruption of genes corA, mgtA, and mgtB, the three major Mg^{2+} influx systems of *Salmonella*. Compared with normal strains that can grow at $[Mg^{2+}]_e$ of 10–100 μmol liter^{-1}, this

strain requires $[Mg^{2+}]_e$ from 10 to 100 mmol liter^{-1} to proliferate (24, 28). We tested the ability of hSLC41A1 to complement the Mg^{2+}-dependent growth-deficient phenotype of strain MM281 by transforming it with plasmids *pUC18-hSLC41A1* or *pUC18-(empty)*.

The expression of His-hSLC41A1 after addition of IPTG (0.02 to 0.05 mmol liter^{-1}) was confirmed by Western blot analysis of the total protein isolate as well as of the immunoprecipitated His-hSLC41A1 from the bacterial membrane protein fraction (Fig. 3). Growth curves were established within 24 h for strains MM281-*pUC18-(empty)*, MM281-*pUC18-hSLC41A1*, and MM1927 in media containing 10 μmol liter^{-1}, 100 μmol liter^{-1}, or 10 mmol liter^{-1} Mg^{2+}. The growth maxima of strains MM1927 and MM281-*pUC18-hSLC41A1* were almost identical at $[Mg^{2+}]_e$ of 10 mmol liter^{-1}, whereas the growth maximum of strain MM281-*pUC18-(empty)* was ~33% lower in comparison with the growth maximum of strain MM1927 (Fig. 4*A*). The growth maximum of strain MM281-*pUC18-hSLC41A1* reached 43% of the growth maximum of strain MM1927 when cultivated at an $[Mg^{2+}]_e$ of 100 μmol liter^{-1} (Fig. 4*B*) and 32.5% when cultivated at an $[Mg^{2+}]_e$ of 10 μmol liter^{-1} (Fig. 4*C*). Strain MM281-*pUC18-(empty)* did not grow in media supplemented with an $[Mg^{2+}]_e$ of 10 or 100 μmol liter^{-1}. As shown in Fig. 4, images of the plated serial dilutions obtained after 24 h of incubation at 37 °C clearly corresponded to the respective sets of the growth curves.

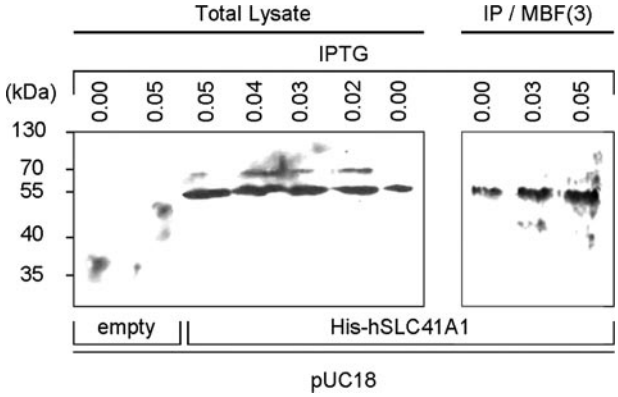

FIGURE 3. **Overexpression of His-hSLC41A1 (56 kDa) in *Salmonella* strain MM281.** His-tagged protein was immunodetected with His_6 tag: GAM-HRP antibodies, or His_6 tag: GAM-κ-HRP antibodies. Bands corresponding to recombinant His-hSLC41A1 immunodetected in total protein isolate and to His-hSLC41A1 immunoprecipitated (*IP*) from the third (ProteoExtract™) membrane-protein-enriched fraction (IP/MBF3) of MM281 bacteria are shown. Expression of His-hSLC41A1 from *pUC18-hSLC41A1* was induced by addition of IPTG at concentrations indicated in the figure. Protein samples were resolved by 12.5% SDS-PAGE.

Furthermore, we measured the $[Mg^{2+}]_i$ of bacteria from strains MM1927, MM281-*pUC18-(empty)*, and MM281-*pUC18-hSLC41A1* by using mag-fura 2 fast filter spectroscopy (27). Mg^{2+}-starved bacteria were incubated in 0.9% saline containing 0 or 10 mmol liter^{-1} Mg^{2+} and the $[Mg^{2+}]_i$ was determined over 20 min. The results are summarized in Fig. 4*D*. The basal $[Mg^{2+}]_i$ measured in Mg^{2+}-free solution was 0.91 ± 0.04, 0.93 ± 0.07, and 0.87 ± 0.03 mmol liter^{-1} in MM1927, MM281-*pUC18-(empty)*, and MM281-*pUC18-hSLC41A1* bacteria, respectively. In MM1927 and MM281-*pUC18-hSLC41A1* bacteria an 89.5 and 42.2% increase of $[Mg^{2+}]_i$ was observed after increasing the $[Mg^{2+}]$ of the external solution to 10 mmol liter^{-1}. In contrast, no change of $[Mg^{2+}]_i$ was measured in strain MM281-*pUC18-(empty)*.

The mag-fura 2 data are in agreement with our results obtained by using ICP-MS. With this technique, the relative

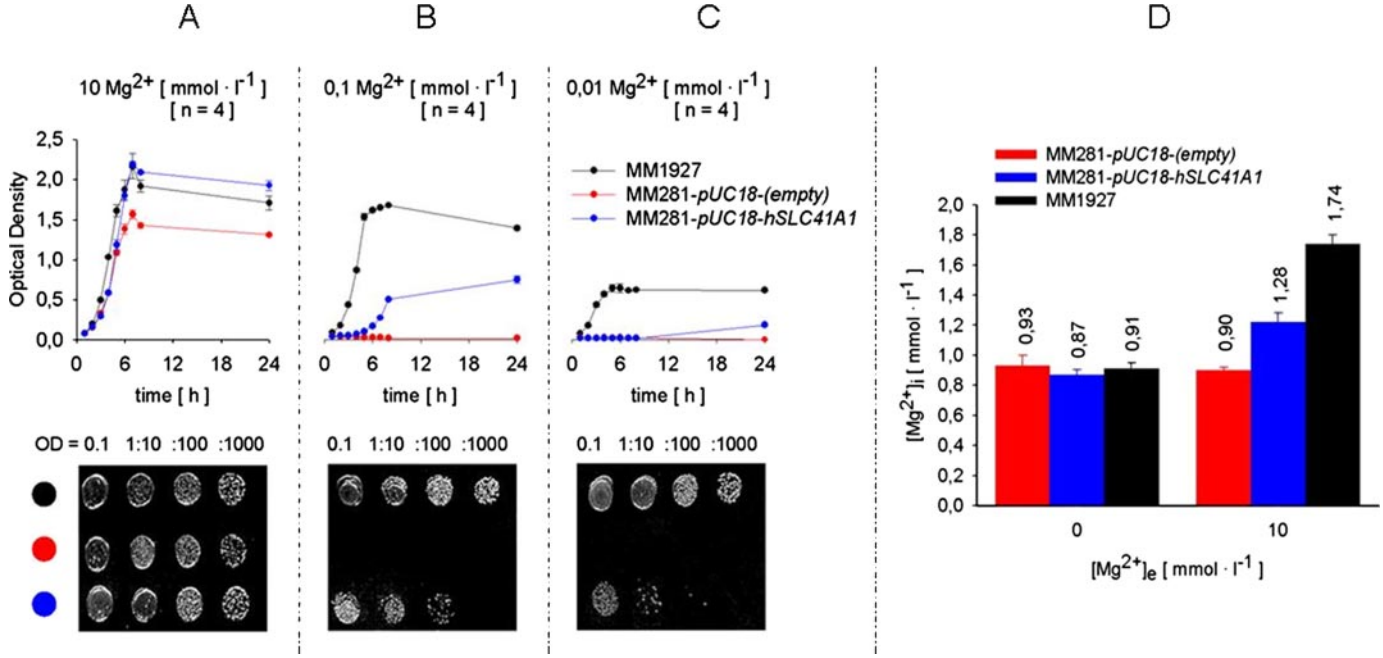

FIGURE 4. **Effect of hSLC41A1 overexpression in *Salmonella*.** Growth curves of *Salmonella* strains MM1927, MM281 transformed with *pUC18-(empty)*, and MM281 transformed with *pUC18-hSLC41A1* grown in N-minimal medium supplemented with 10 mmol liter^{-1} (*A*), 100 μmol liter^{-1} (*B*), or 10 μmol liter^{-1} (*C*) $MgCl_2$. Growth curves averaged from three independent experiments for each respective $[Mg^{2+}]_e$ and corresponding serial dilutions (*bottom*) plated on the solid N-minimal medium are shown. *D*, steady-state $[Mg^{2+}]_i$ of bacteria from strains MM1927, MM281 transformed with *pUC18-(empty)*, and MM281 transformed with *pUC18-hSLC41A1* measured after a 20-min incubation in nominally Mg^{2+}-free or 10 mmol liter^{-1} Mg^{2+} containing saline. Mean ± S.E. of three to four independent experiments are given. *OD*, optical density.

increase of the total magnesium concentration ($\Delta[Mg]_t$) for bacteria grown 24 h at an $[Mg^{2+}]_e$ of 2 mmol liter^{-1} and those grown at an $[Mg^{2+}]_e$ of 10 mmol liter^{-1} was established for all three strains. The $\Delta[Mg]_t$ for MM281-*pUC18-hSLC41A1* was 14.2%, similar to the 16.7% $\Delta[Mg]_t$ measured in MM1927. The $\Delta[Mg]_t$(MM281-*pUC18-*(*empty*) remained at 7.3% and was significantly less than the $\Delta[Mg]_t$ determined for strains MM1927 and MM281-*pUC18-hSLC41A1*.

Patch Clamp Characterization of hSLC41A1—Using TEV, Goytain and Quamme (15) observed large Mg^{2+} currents associated with mouse SLC41A1 when overexpressed in *X. laevis* oocytes. Therefore, we expected Mg^{2+} carried currents to appear after hSLC41A1 overexpression in HEK293 cells. To characterize such currents, patch clamp experiments in the whole cell configuration with +tet (15–18 h) and non-induced HEK293-(SLC41A1) cells were performed. Repetitive voltage ramps that spanned −100 to +100 mV over 50 ms were delivered every 2 s from a holding potential of 0 mV. Inward currents were assessed at −80 mV and outward currents at +80 mV. An inwardly directed Mg^{2+} concentration gradient was created by perfusion of cells with Mg^{2+}-free internal saline (K^+-Glu-based, if not stated otherwise), whereas the external solution contained 2 mmol liter^{-1} Mg^{2+}. Under these experimental conditions, development of a small but identifiable current at negative membrane potentials (−100 to 0 mV) would be predicted in SLC41A1 overexpressing cells that would not be seen in non-induced cells. This current would be expected to have a more positive reversal potential (E_{rev}) and would be carried by Mg^{2+}. Instead, SLC41A1 overexpressing cells developed a large outwardly rectifying conductance (Fig. 5*A*). This current was fully activated within 200 s of the experiment and its current-voltage (I-V) relationship (Fig. 5*B*) revealed a highly nonlinear current with a reversal potential of around −35 mV. The development of the SLC41A1-induced current could be prevented in the presence of 1 mmol liter^{-1} intracellular Mg^{2+} (Fig. 5, *C* and *D*).

To test whether the SLC41A1-induced conductance could support Mg^{2+} influx, cells were initially bathed in the standard external solution containing 1 mmol liter^{-1} Ca^{2+} and 2 mmol liter^{-1} Mg^{2+}. At 200 s, when the SLC41A1-induced conductance had reached its full amplitude, an isotonic solution of 115 mmol liter^{-1} Mg^{2+} was applied for 60 s via a buffer pipette (Fig. 5*E*). This had no significant effect on either inward or outward currents, and the shape of the I-V relationship extracted at the end of the application was also not affected compared with the control (data not shown). In conclusion these unexpected results clearly show that the SLC41A1-induced conductance did not give rise to an Mg^{2+} influx but exhibited typical characteristics of a chloride conductance.

Therefore, further experiments were set out to confirm the latter. To this end, we allowed the current to develop fully before applying an external solution supplemented with 100 μmol liter^{-1} of the Cl^- channel inhibitor DIDS. This resulted in a fast and almost complete block of the current (Fig. 5, *F* and *G*). In control experiments with +tet (15–18 h) HEK293-(TRPM7) cells, the application of 100 μmol liter^{-1} DIDS had no effect on TRPM7 current (data not shown).

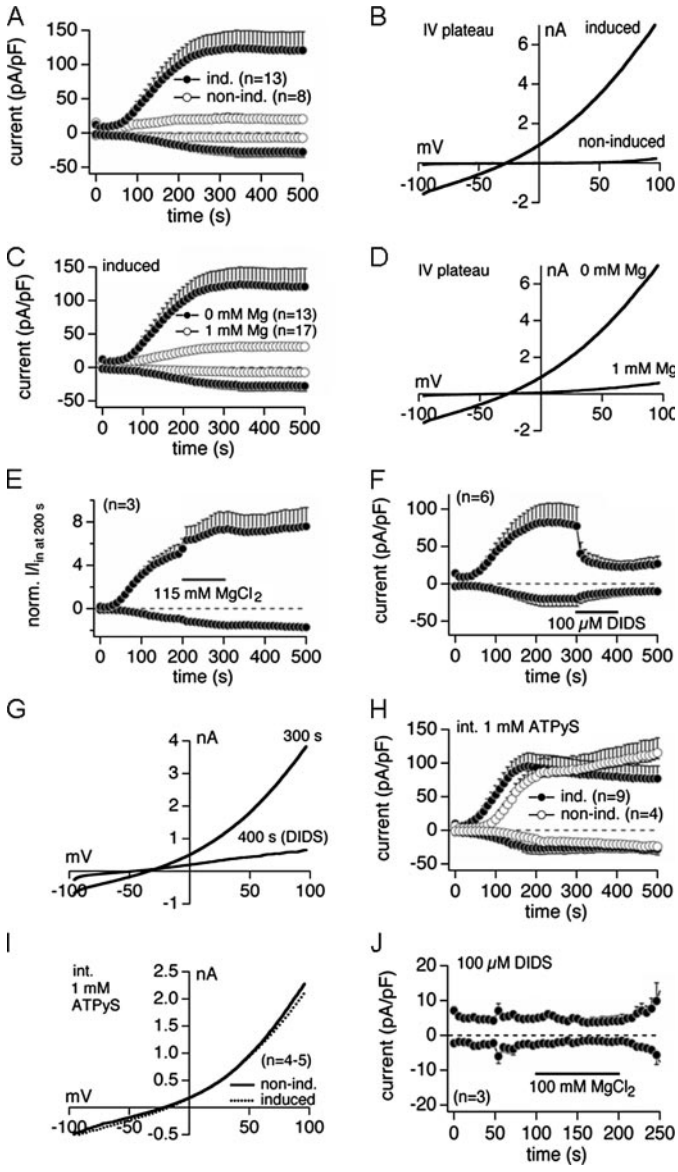

FIGURE 5. **Electrophysiological characterization of hSLC41A1 related current in HEK293-(SLC41A1) cells (*ind.*, induced; *non-ind.*, non-induced).** *A*, average current densities at −80 and +80 mV induced by Mg^{2+}-free internal saline in +tet (15–18 h) and −tet HEK293-(SLC41A1) cells. *B*, examples of current-voltage (*I-V*) relationships at plateau current in +tet and −tet cells extracted from experiments shown in *A*. *C*, average current densities at −80 and +80 mV induced by Mg^{2+}-free internal saline in +tet (15–18 h) HEK293-(SLC41A1) cells compared with average current densities induced by internal saline containing 1 mmol liter^{-1} Mg^{2+} in +tet (15–18 h) HEK293-(SLC41A1) cells. *D*, examples of current-voltage (I-V) relationships at the plateau current in +tet cells perfused with Mg^{2+}-free or 1 mmol liter^{-1} Mg^{2+} internal solution extracted from experiments shown in *C*. *E*, average normalized currents at −80 and +80 mV induced by Mg^{2+}-free internal saline in +tet (15–18 h) HEK293-(SLC41A1) cells. From t = 200 to 300 s, 115 mmol liter^{-1} $MgCl_2$ was applied externally via an application pipette. Inward and outward currents were normalized to the current size at −80 mV after 200 s (immediately before application of 115 mmol liter^{-1} $MgCl_2$). *F*, average current densities at −80 and +80 mV induced by Mg^{2+}-free internal saline in +tet cells. 100 μmol liter^{-1} DIDS was applied externally via application pipette from t = 300 to 400 s. *G*, examples of I-V relationships of the current before (at 300 s) and at the end (at 400 s) of a 100 μmol liter^{-1} DIDS application. Traces are extracted from experiments shown in *D*. *H*, average current densities at −80 and +80 mV induced by internally applied 1 mmol liter^{-1} ATPγS in +tet and −tet cells. *I*, average I-V relationships at plateau current in +tet and −tet cells extracted from experiments shown in *F*. *J*, average current densities at −80 and +80 mV induced by Mg^{2+}-free internal saline (buffered with 10 mmol liter^{-1} HEDTA) in the presence of 100 μmol liter^{-1} external DIDS in +tet cells. 100 mmol liter^{-1} $MgCl_2$ was applied externally via application pipette from t = 100 to 200 s.

In the next set of experiments we used Mg^{2+}-free KCl-based instead of K^+-Glu-based internal saline. Under these conditions we observed: 1) an inward current that could not be seen when K^+-Glu buffer was used for perfusion of +tet HEK293-(SLC41A1) cells (data not shown) and 2) a depolarizing shift of the E_{rev} as predicted for Cl^- conductance by the Nernst equation (data not shown). At 300 s, a low Cl^- solution was applied for 100 s via a buffer pipette. As expected, this resulted in a strong reduction of the outward current during application, whereas the inward current remained the same (data not shown). The application of low Cl^- solution also evoked a further depolarizing shift of the E_{rev} (data not shown). These data in conjunction with the DIDS sensitivity of the current clearly confirm the involvement of Cl^- channels.

Because some Cl^- channels are activated by protein phosphorylation (33, 34) we wished to determine whether the SLC41A1-induced conductance would also be activated. To this end, we perfused both −tet and +tet cells with a Mg^{2+}-free intracellular solution supplemented with 1 mmol $liter^{-1}$ ATPγS, a non-hydrolysable substrate for ATPases. In −tet cells, ATPγS gave rise to a Cl^- conductance that was identical to the conductance and I-V curves seen in +tet cells in the absence of this substrate (Fig. 5*H*). Moreover, ATPγS did not cause recruitment of any additional currents in SLC41A1-overexpressing cells (Fig. 5, *A versus H* and *I*) and the ATPγS-induced currents developed in an identical manner even in the complete absence of intracellular and extracellular Mg^{2+} (data not shown). We wondered whether suppression of the SLC41A1-induced Cl^- conductance would reveal any Mg^{2+} influx that might have been masked by the large currents that develop in +tet cells. However, upon suppression of the Cl^- currents by supplementing the extracellular solution with 100 μmol $liter^{-1}$ DIDS and superfusing the cells with an isotonic Mg^{2+} solution, no further Mg^{2+} influx could be detected (Fig. 5*J*).

It is known that two molecules of tetracycline can chelate one Mg^{2+} (30). To exclude any tetracycline effects on our measurements, wild type (WT) HEK293 cells grown for 15 h in tetracycline-containing medium (1 μg/ml) were perfused with Mg^{2+}-free internal saline and examined in whole cell mode patch clamp experiments. As predicted, no conductance similar to that measured in SLC41A1 overexpressing HEK293 cells was found in WT cells grown in +tet medium (data not shown).

Functional Characterization of hSLC41A1 in HEK293 Cells by Use of mag-fura 2—Because of the sequence homology of SLC41A1 to the bacterial Mg^{2+} transporter MgtE, we wondered whether this protein might be involved in Mg^{2+} transport functioning as a carrier protein rather than an ion channel mechanism. We therefore set out to measure intracellular Mg^{2+} concentrations by using a mag-fura 2-based ratiometric assay. HEK293 cells bearing FLAG-tagged SLC41A1 were induced for 5, 10, or 15 h with tetracycline and, afterward, the $[Mg^{2+}]_i$ was measured over a 20-min period in media with an $[Mg^{2+}]_e$ of 0, 2, 5, or 10 mmol $liter^{-1}$. The −tet HEK293-(SLC41A1) cells were used in control experiments. Representative original recordings of $[Mg^{2+}]_i$ measurements in +tet (15 h) and −tet cells are shown in Fig. 6*A*. In Table 1, $[Mg^{2+}]_i$ values determined at the end of the measuring period are summarized for all conditions.

The incubation of +tet HEK293-(SLC41A1) cells in completely Mg^{2+}-free medium always led to a significant decrease of their $[Mg^{2+}]_i$ compared with that of −tet HEK293-(SLC41A1) cells (Fig. 6, *A* and *B*, and Table 1). The lower end point $[Mg^{2+}]_i$ of +tet HEK293-(SLC41A1) cells resulted from a continuous decrease of their $[Mg^{2+}]_i$ during the measuring period, amounting to 41 ± 8, 124 ± 38, and 149 ± 18 μmol $liter^{-1}$ per 20 min after 5, 10, and 15 h of induction, respectively (Fig. 6*B*). Such a process was never seen in −tet HEK293-(SLC41A1) cells or wild type HEK293 cells, which showed a negligible (56 ± 7 μmol $liter^{-1}$) $[Mg^{2+}]_i$ increase under these conditions. These surprising results point to an increased efflux capacity of HEK293 cells overexpressing SLC41A1.

Compared with the zero-Mg^{2+} conditions, higher $[Mg^{2+}]_i$ values were observed in both +tet and −tet cells if they were incubated in Mg^{2+}-containing medium (Fig. 6*A* and Table 1). However, from 10 h and more after induction, +tet HEK293-(SLC41A1) cells had a significantly higher $[Mg^{2+}]_i$ at the end of the measuring period than −tet cells at all $[Mg^{2+}]_e$ used (Table 1). In contrast, no $[Mg^{2+}]_i$ increase was observable in the presence of transmembrane Ca^{2+} gradients favoring calcium influx (Fig. 6*A*). Control measurements performed by use of fura 2 showed that hSLC41A1 overexpression and/or increasing the extracellular $[Ca^{2+}]$ from 2 to 10 mmol $liter^{-1}$ induced no elevation of the free cytosolic $[Ca^{2+}]$ ($[Ca^{2+}]_i$). The mean $[Ca^{2+}]_i$ determined at the end of the measuring period always amounted to 128 ± 4 nmol $liter^{-1}$. Again, a possible effect of tetracycline traces on the $[Mg^{2+}]_i$ changes was tested in +tet (10 and 15 h) HEK293 WT cells. The results are summarized in Table 1 showing that the $[Mg^{2+}]_i$ of −tet or +tet wt HEK293 cells was not different from that measured in −tet HEK293-(SLC41A1) cells.

Because the patch clamp data revealed an inhibition of the SLC41A1-related Cl^- conductance in +tet HEK293-(SLC41A1) cells treated with 100 μmol $liter^{-1}$ DIDS (Fig. 5, *F* and *G*), we investigated whether this inhibitor also influenced their $[Mg^{2+}]_i$. As shown in Fig. 6*C*, this was not the case and the $[Mg^{2+}]_i$ of +tet cells treated with the non-fluorescent H_2-DIDS (100 μmol $liter^{-1}$) was not different from that of untreated control cells.

In −tet HEK293-(SLC41A1) cells, the $[Mg]_i$ increase was solely dependent on the extracellular $[Mg^{2+}]$ in a linear ($\Delta[Mg^{2+}] = 187.8 + 94.5[Mg^{2+}]_e$; $r^2 = 0.99$) manner (Fig. 6*D*). After correction for this linear component, a $[Mg^{2+}]_i$ elevation was still observable in +tet HEK293-(SLC41A1) cells (Fig. 6*E*). This remaining component was assumed to result mainly from SLC41A1 overexpression and its extent was dependent on $[Mg^{2+}]_e$ and on the duration of tet-induction (Fig. 6*E*). It showed an apparent saturation after 10 h of induction when it amounted to about 250 μmol $liter^{-1}$ per 20 min, but a maximum of 412 ± 30 μmol $liter^{-1}$ per 20 min was observed 15 h after induction and with 10 mmol $liter^{-1}$ of $[Mg^{2+}]_e$. The $[Mg^{2+}]_i$ increase observed under the latter conditions showed strong temperature sensitivity. In the experiments summarized in Fig. 7*A*, media temperatures were held at 37 (control), 25, or 40 °C during the 20-min measurement period. Reduction or

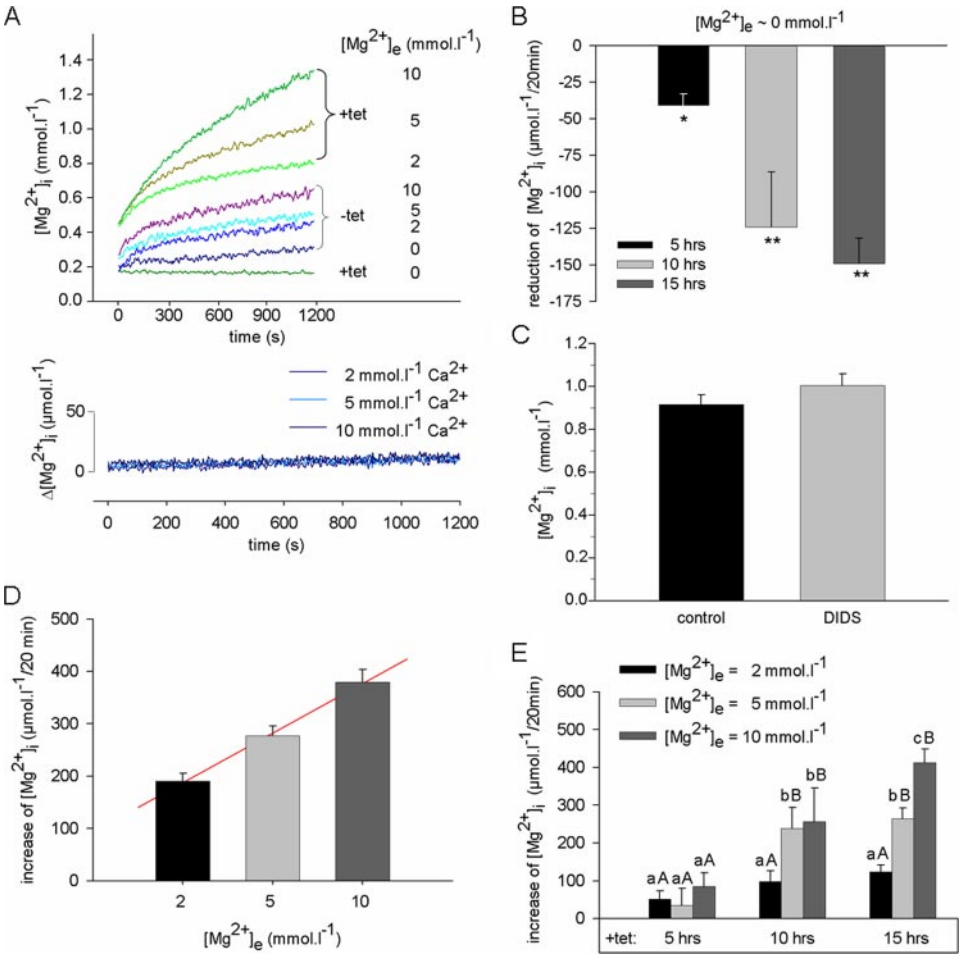

FIGURE 6. **Effect of hSLC41A1 overexpression on the free intracellular Mg^{2+} concentration ($[Mg^{2+}]_i$) of HEK293 cells.** *A*, representative original recordings for $[Mg^{2+}]_i$ of −tet and +tet (15 h) HEK293-(SLC41A1) cells at various $[Mg^{2+}]_e$ and $[Ca^{2+}]_e$. Note the continuous $[Mg^{2+}]_i$ decrease in +tet HEK293-(SLC41A1) cells during exposure to Mg^{2+}-free medium. *B*, summary of results showing SLC41A1-dependent reduction of $[Mg^{2+}]_i$ after incubation of +tet HEK293-(SLC41A1) cells in Mg^{2+}-free medium. Mean $[Mg^{2+}]_i$ decrease after 20 min exposure to completely Mg^{2+}-free is shown. Values are mean ± S.E. of five to eight single experiments. *, $p < 0.05$ *versus* −tet cells; **, $p < 0.01$ *versus* −tet cells. *C*, influence of H_2DIDS on $[Mg^{2+}]_i$ of +tet (15 h) HEK293-(SLC41A1) cells. Steady-state $[Mg^{2+}]_i$ values measured 20 min after suspending cells in solutions containing 10 mmol liter^{-1} Mg^{2+} are shown for H_2DIDS-treated and control cells. Values are mean ± S.E. of seven single experiments. *D*, $[Mg^{2+}]_i$ changes in −tet HEK293-(SLC41A1) cells exposed to inwardly directed Mg^{2+} gradients. Mean $[Mg^{2+}]_i$ changes after 20 min exposure to solutions containing 2, 5, or 10 mmol liter^{-1} Mg^{2+} are shown. *Line* is fitted to data by linear regression analysis (parameters: $y_0 = 187.8$, $a = 94.5$; $r^2 = 0.99$). Data are given as mean ± S.E. of six single experiments. *E*, SLC41A1-dependent increase of $[Mg^{2+}]_i$ after exposure of +tet (5, 10, and 15 h) HEK293-(SLC41A1) cells to inwardly directed Mg^{2+} gradients. Mean $[Mg^{2+}]_i$ changes determined after 20 min exposure to solutions containing 2, 5, or 10 mmol liter^{-1} Mg^{2+} and corrected for the increase observed in parallel measurements with −tet HEK293-(SLC41A1) cells are given. Values are mean ± S.E. of six single experiments. Within an induction time, means that do not have a common *lowercase letter* differ, $p < 0.05$; within a $[Mg^{2+}]_e$, means that do not have a common *uppercase letter* differ, $p < 0.05$.

elevation of the temperature significantly decreased (0.33 ± 0.03 mmol liter^{-1}) or increased (1.29 ± 0.06 mmol liter^{-1}) the end point $[Mg^{2+}]_i$ of SLC41A1 overexpressing cells when compared with that (0.95 ± 0.03 mmol liter^{-1}) observed in control cells. This corresponded to changes in the apparent Mg^{2+} accumulation that amounted to 569 ± 20, 79 ± 7, and 737 ± 54 μmol liter^{-1} when cells were measured under control, low, or high temperature conditions, respectively (Fig. 7*A*).

Next, we wished to determine whether the observed $[Mg^{2+}]_i$ changes were accompanied by net changes of $[Mg]_t$ (measured by atomic mass spectroscopy). In these experiments, all cells were pre-starved in Mg^{2+}-free medium for 60 min (this time was adequate for mag-fura 2 AM loading and activation in the fast filter spectroscopy measurements described above) and then incubated in the presence of 10 mmol liter^{-1} Mg^{2+} over a time period of 20 min. As shown in Fig. 7*B*, the $[Mg]_t$ of −tet HEK293-(SLC41A1) cells was not influenced by incubation in Mg^{2+}-free or high-Mg^{2+} (10 mmol liter^{-1}) medium. However, when +tet (5 h) HEK293-(SLC41A1) cells were kept in Mg^{2+}-free medium, their $[Mg]_t$ decreased by 25.6% compared with that of −tet cells incubated under the same conditions. Again, such results are only explainable by an increased SLC41A1-mediated Mg^{2+} efflux from these cells. When Mg^{2+} (10 mmol liter^{-1}) was present during the 20-min incubation time, the $[Mg]_t$ of these cells increased by

TABLE 1

$[Mg^{2+}]_i$ (mmol liter^{-1}) of non-induced (−tet) and induced (+tet) HEK293-(SLC41A1) cells and +tet HEK293 wild type (WT) cells measured at various $[Mg^{2+}]_e$

$[Mg^{2+}]_i$ values achieved after 20 min in the respective medium are given. Data are presented as mean ± S.E. of 4–15 single experiments.

$[Mg^{2+}]_e$	−tet	+tet				
		HEK293-(SLC41A1)			HEK293 (WT)	
		5 h	10 h	15 h	10 h	15 h
mmol liter^{-1}						
0	0.39 ± 0.03	0.16 ± 0.02[a]	0.22 ± 0.01[b]	0.10 ± 0.03[b]	0.34 ± 0.02	0.38 ± 0.07
2	0.47 ± 0.02	0.49 ± 0.02	0.67 ± 0.05[a]	0.72 ± 0.03[a]	0.39 ± 0.06	0.44 ± 0.02
5	0.58 ± 0.02	0.60 ± 0.03	0.96 ± 0.08[a]	0.99 ± 0.03[a]	0.47 ± 0.05	0.51 ± 0.02
10	0.73 ± 0.02	0.83 ± 0.03[b]	0.98 ± 0.15[b]	1.04 ± 0.08[a]	0.56 ± 0.11	0.68 ± 0.03

[a] $p < 0.01$ *versus* control (−tet).
[b] $p < 0.05$ *versus* control (−tet).

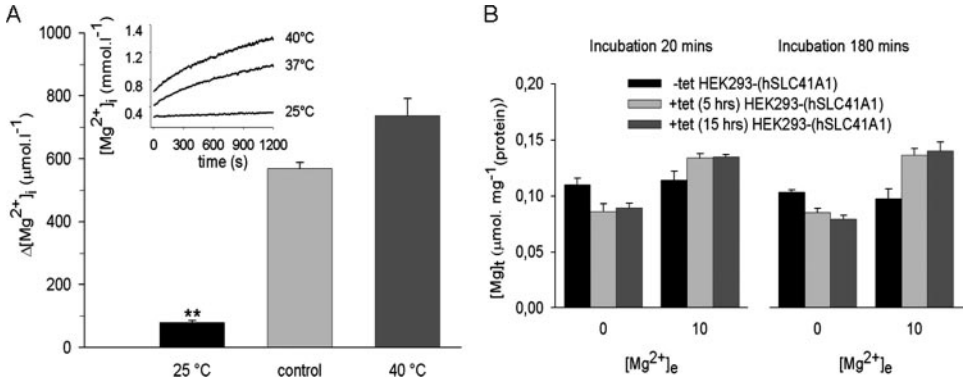

FIGURE 7. *A*, temperature sensitivity of SLC41A1-related $[Mg^{2+}]_i$ changes in HEK293-(SLC41A1) cells. $[Mg^{2+}]_i$ changes were measured in +tet (15 h) HEK293-(SLC41A1) cells incubated in media containing 10 mmol liter^{-1} Mg^{2+}. Medium temperatures were held at 37, 25, or 40 °C. $[Mg^{2+}]_i$ increases obtained after 20 min exposure to the respective temperature condition are given. The *inset* shows representative original $[Mg^{2+}]_i$ recordings. Values are mean ± S.E. of five to seven single experiments. **, $p < 0.01$ *versus* control (37 °C). *B*, $[Mg]_t$ determined in −tet and +tet (5 h and 15 h) HEK293-(SLC41A1) cells incubated in Mg^{2+}-free HEK293 medium and in HEK293 medium supplemented with 10 mmol liter^{-1} Mg^{2+}. Sets of $[Mg]_t$ values determined after 20 and 180 min incubation at these $[Mg^{2+}]_e$ are shown. Values are mean ± S.E. averaged from three independent measurements.

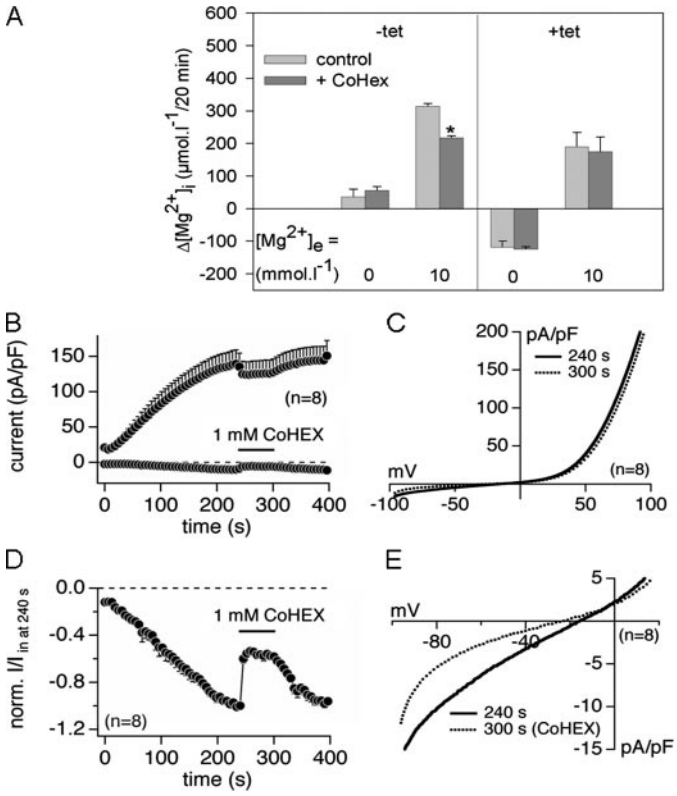

FIGURE 8. **Effects of the Mg^{2+} channel inhibitor CoHex on SLC41A1 and TRPM7 Mg^{2+} transport.** *A*, summary of the CoHex effect on the $[Mg^{2+}]_i$ of −tet and +tet (15 h) HEK293-(SLC41A1) cells incubated in either Mg^{2+}-free or Mg^{2+}-containing (10 mmol liter^{-1}) medium. Mean $[Mg^{2+}]_i$ changes (−tet cells) and mean $[Mg^{2+}]_i$ changes corrected as described in the legend to Fig. 5*E* (+tet cells) are shown. Values are mean ± S.E. of three single experiments. *, $p < 0.05$ *versus* control cells (without CoHex). *B*, average current densities at −80 and +80 mV induced by Mg^{2+}-free (+10 mmol liter^{-1} BAPTA) internal saline in +tet (14–20 h) HEK293-(TRPM7). 1 mmol liter^{-1} CoHex was applied via an application pipette during the time course of 60 s (from 240 to 300 s). *C*, averaged I-V relationships extracted from experiments shown in *B* at the current plateau before (at 240 s) and during (at 300 s) application of 1 mmol liter^{-1} CoHex. *D*, average inward current at −80 mV shown in *B* normalized to the current size immediately before application of 1 mmol liter^{-1} CoHex (I/I in at 240 s). *E*, extracted part of the I-V depicted in *C*, showing the ~50% inhibition of the TRPM7 inward current by 1 mmol liter^{-1} CoHex.

+12.7% indicating replenishment of the intracellular Mg^{2+} stores by another mechanism than SLC41A1. The same results were observed after an extension of the *hSLC41A1* induction period to 15 h.

Furthermore, we tested whether extension of the Mg^{2+} starvation and/or loading time would led to a further decrease and/or increase of $\Delta[Mg]_t$ in +tet HEK293-(SLC41A1) cells. Increasing the incubation time in 0 mM Mg^{2+} medium from 20 to 180 min reduced $[Mg]_t$ by 15.4 (5 h +tet) and 21.7% (15 h +tet), respectively. A prolongation of the Mg^{2+} loading time, however, resulted in an 32.6 (5 h +tet) and 37.9% (15 h +tet) $[Mg]_t$ increase, respectively (Fig. 7*B*).

Effect of the Mg^{2+} Channel Inhibitor Cobalt(III) Hexaammine on the $[Mg^{2+}]_i$ of +tet (15 h) HEK293-(SLC41A1) Cells and on TRPM7-mediated Mg^{2+} Conductance—To differentiate channel- and carrier-mediated transport components, we next determined whether the only known inhibitor of channel-mediated Mg^{2+} transport (13, 35) cobalt(*III*) hexaammine (CoHex) influenced the $[Mg^{2+}]_i$ of +tet (15 h) HEK293-(SLC41A1) cells incubated in media containing 0, 2, 5, or 10 mmol liter^{-1} $MgCl_2$. No significant effect of 1 mmol liter^{-1} CoHex was seen in Mg^{2+}-free medium. However, in media with 2, 5, or 10 mmol liter^{-1} Mg^{2+}, the end point $[Mg^{2+}]_i$ of CoHex-treated cells was reduced by 134 ± 8, 162 ± 10, and 254 ± 9 μmol liter^{-1}, respectively, compared with that measured in non-treated control cells. Thus, a CoHex-sensitive component was observable in the presence of extracellular Mg^{2+} only and amounted to about 25% at each $[Mg^{2+}]_e$. Therefore, in another series of experiments, the effects of CoHex on $[Mg^{2+}]_i$ changes were compared for −tet and +tet (15 h) HEK293-(SLC41A1) cells incubated in either totally Mg^{2+}-free or 10 mM Mg^{2+} medium (Fig. 8*A*). In −tet cells incubated in 0 mmol liter^{-1} Mg^{2+} medium, CoHex had no significant effect on the $[Mg^{2+}]_i$ but the inhibitor led to a significant 30% reduction of $[Mg^{2+}]_i$ in 10 mmol liter^{-1} Mg^{2+} medium (Fig. 8*A*). In contrast, the SLC41A1-related $[Mg^{2+}]_i$ change was not influenced by CoHex (Fig. 8*A*). These data confirm the existence of a CoHex-blockable Mg^{2+} influx mechanism(s) not identical to SLC41A1 in HEK293 cells. A likely candidate for such a transport mechanism is the TRPM7 ion channel, which is endogenously expressed in this cell type (36). To study the effect of CoHex on TRPM7 current development, we performed patch clamp experiments in the whole cell configuration mode with +tet (14–20 h) HEK293-(TRPM7) cells (12). CoHex was applied 60 s after the start of the experiment when TRPM7 currents were fully developed. CoHex at 1 mmol liter^{-1} reversibly blocked inward TRPM7 currents (relevant to divalent cations, mainly Mg^{2+} conductance) by 51.3 ± 1.8%, whereas outward TRPM7 currents (relevant to monovalent ion con-

ductance) remained almost unaffected (12.3 ± 0.6% inhibition) in the presence of 2 mmol liter^{-1} $[Mg^{2+}]_e$ (Fig. 8, *B–E*).

DISCUSSION

At present, our understanding of the molecular identity and cellular functions of SLC41A1 is limited. The sequential similarity between SLC41A1 and the putative bacterial Mg^{2+} transporter MgtE (14) and the up-regulation of SLC41A1 expression in response to a low Mg^{2+} diet (15) lead to the hypothesis that SLC41A1 is involved in Mg^{2+} homeostasis and/or Mg^{2+} transport in cells of higher eukaryotes. This hypothesis is supported by our data showing the functional substitution of CorA, MgtA, and MgtB Mg^{2+} transporters by hSLC41A1 in the *Salmonella* strain MM281. Moreover, the results described here provide experimental evidence that SLC41A1, the first molecularly characterized Mg^{2+} carrier in eukaryotes, probably mediates Mg^{2+} efflux. The basis for this conclusion is 4-fold: 1) overexpression of SLC41A1 in HEK293 cells does not induce detectable Mg^{2+}-carried currents, 2) in Mg^{2+}-free media, SLC41A1 overexpression leads to a significant reduction of $[Mg^{2+}]_i$ and $[Mg]_t$, 3) the intensity of the Mg^{2+} loss depends on the induction time and thus on the number of SLC41A1 molecules in the cell membrane, and 4) SLC41A1-related $[Mg^{2+}]_i$ changes are temperature-sensitive but not influenced by the Mg^{2+} channel blocker CoHex.

hSLC41A1 Functionally Complements Disruption of the CorA-MgtA-MgtB Transport System in S. enterica sv. typhymurium—The Mg^{2+}-dependent growth-deficient *Salmonella* strain MM281 represents, with certain limitations, a simple model for testing the ability of the candidate Mg^{2+} transporters to restore its growth and thus to identify the direct involvement of these transporters in Mg^{2+} transport (24, 37, 38). *SLC41A1* has only been identified in the genomes of eukaryotes (14, 15), however, due to its distant sequential ancestry with the bacterial MgtE, we reasoned that it might be able to complement the growth-deficient phenotype of the MM281 strain. MgtE can mediate Mg^{2+} uptake in bacteria but lacks homology to the other known bacterial Mg^{2+} transporters as it does not possess the typical F/YGMN motif, which is characteristic for members of the CorA-Mrs2-Alr1 superfamily of Mg^{2+} transporters (13). Nevertheless, as our data show, hSLC41A1, when overexpressed from *pUC18-hSLC41A1* in the MM281 strain, partly restores the growth of this triple disruption of *Salmonella* in low Mg^{2+} media. However, the growth-promoting effect of SLC41A1 is less than that of Mrs2 (13). The latter is present in the mitochondria of the eukaryotes and represents a distant homologue of the bacterial Mg^{2+} channel CorA. Functional complementation by SLC41A1 corresponds well to our data obtained by ICP-MS demonstrating a significant increase of the total magnesium concentration in the MM281 strain transformed with *pUC18-hSLC41A1* in comparison with the $[Mg]_t$ in the MM281 strain transformed with *pUC18-(empty)*. The ability of hSLC41A1 to complement the Mg^{2+}-linked growth-deficient phenotype of *Salmonella* strain MM281 identifies hSLC41A1 as being a *bona fide* Mg^{2+} transporter.

hSLC41A1 Probably Forms Hetero-oligomeric Complexes in a Mammalian Expression System—Taking into account that hSLC41A1 maintains its functionality when expressed in *Salmonella* and that the *Salmonella* genome lacks mgtE, hSLC41A1 probably works as a monomer and/or a homo-oligomer in this expression system. However, various solute transporters have been shown to form stable or transient protein complexes to become functional in their native systems (31, 32). This is in agreement with our findings establishing that SLC41A1 forms protein complexes of "high" molecular mass (~1000 kDa) when overexpressed in HEK293 cells. In addition, our two-dimensional PAGE data indicate the presence of distinct proteins in the observed SLC41A1 complexes, further suggesting the hetero-oligomeric character of SLC41A1 complexes in the mammalian system. SLC41A2 and SLC41A3 are possible candidates for being binding partners in such complexes. This hypothesis is indirectly supported by our recent observation that all three genes are being overexpressed simultaneously in response to extracellular Mg^{2+} starvation in lymphocytes.[7] Even so, protein(s) other than SLC41A2 or SLC41A3 (*e.g.* protein components of the cytoskeleton, other ion transporters, and/or enzymes) must be integrated in SLC41A1-containing complexes to reach the observed molecular masses between 720 and 1236 kDa. Future studies investigating SLC41A1-binding partners and the composition of the SLC41A1 complexes in response to specific physiological conditions will clarify this.

hSLC41A1 Overexpression Does Not Induce Measurable Mg^{2+} Currents, but Allows Mg^{2+} Efflux and Is Associated with an Endogenous Cl^- Conductance—Overexpression of mSLC41A1 in *X. laevis* oocytes has been shown to induce large Mg^{2+}-carried currents, although various other divalent cations are also transported (15). Using TEV, Goytain and Quamme (15) determined the following SLC41A1-specific permeation profile: $Mg^{2+} \geq Sr^{2+} \geq Fe^{2+} \geq Ba^{2+} \geq Cu^{2+} \geq Zn^{2+} \geq Co^{2+} > Cd^{2+}$. However, because of the lack of a control for the intracellular ion milieu, TEV does not allow the establishment of a true permeation profile. Nevertheless, these data suggest that SLC41A1 is an unspecific divalent cation channel. In contrast, the currents induced by SLC41A1 overexpression in our +tet HEK293-(SLC41A1) cells have been identified as endogenous Cl^- currents, recruited by depletion of intracellular Mg^{2+} and blockable by the broad-spectrum Cl^- transport antagonist DIDS. These currents are not affected by changing the driving force for Mg^{2+} across the plasma membrane. In accordance with our data, SLC41A2, another member of the SLC41 transporter family, has also been reported to mediate large Mg^{2+} currents when expressed in *X. laevis* oocytes (16) but induces no significant currents after expression in TRPM7-deficient DT40 cells (17).

Nevertheless, SLC41A1-related Mg^{2+} transport is clearly demonstrated by our results showing changes of the $[Mg^{2+}]_i$ and of the total [Mg] ($[Mg]_t$) in +tet HEK293-(SLC41A1) cells. One of the main differences between −tet and +tet HEK293-(SLC41A1) cells is a significantly lower $[Mg^{2+}]_i$ and $[Mg]_t$ in the

[7] F. Rolle, J. Vormann, M. Schweigel, and M. Kolisek, manuscript in preparation.

latter after incubation in a completely Mg^{2+}-free medium ($[Mg^{2+}]_i > [Mg^{2+}]_e$). This raises the possibility that SLC41A1 mediates Mg^{2+} efflux that is supported by the following findings: 1) the intensity of the observed $[Mg^{2+}]_i$ and $[Mg]_t$ decrease is clearly dependent on the duration of tet-induction and therefore is more pronounced in correlation with the translocation of more SLC41A1 proteins to the cell membrane, and 2) neither WT nor −tet HEK293-(SLC41A1) cells ever develop such a significant $[Mg^{2+}]_i$ or $[Mg]_t$ decrease, even in the absence of extracellular magnesium (Table 1). In contrast, cells with a low SLC41A1 expression show a slight $[Mg^{2+}]_i$ increase and, as no extracellular Mg^{2+} is available under these conditions, the release of the ion from intracellular buffers or organelles might be responsible for this observation. These findings were surprising, because, based on the results of Goytain and Quamme (15), an increased Mg^{2+} influx capacity of +tet HEK293-(SLC41A1) was expected. For this reason, our experiments were originally designed to support such SLC41A1-related Mg^{2+} uptake by performing all preparation and storage procedures before the actual measurements in Mg^{2+}-free solutions. It is very likely that +tet HEK293-(SLC41A1) cells already lose relatively high amounts of intracellular Mg^{2+} during this time period due to increased magnesium efflux compared with wild type cells. This assumption is supported by the very low initial $[Mg^{2+}]_i$ levels (~0.2 mmol liter^{-1}) measured in +tet HEK293-(SLC41A1) cells incubated in Mg^{2+}-free medium.

HEK293 cells express the constitutively active channel TRPM7, which has been shown to mediate Mg^{2+} uptake in various cell types (11, 12, 39). Thus, TRPM7 background activity mainly explains the $[Mg^{2+}]_i$ increase seen in −tet and +tet HEK293-(SLC41A1) cells in the presence of an inwardly directed Mg^{2+} gradient. However, a higher efflux capacity after hSLC41A1 overexpression in conjunction with lower initial $[Mg^{2+}]_i$ levels may result in a stronger TRPM7-mediated influx component in +tet HEK293-(SLC41A1) cells. After correction for this component, an apparent "Mg^{2+} uptake" still persists resulting in an additional increase of $[Mg^{2+}]_i$ and significantly higher end point $[Mg^{2+}]_i$ levels compared with non-induced control cells. At least at the high $[Mg^{2+}]_e$ of 10 mmol liter^{-1}, this is accompanied by a net increase of $[Mg]_t$. Although we cannot preclude from the presented results that SLC41A1 can also mediate Mg^{2+} influx in the presence of strong inside-directed Mg^{2+} gradients, our data suggest a $[Mg^{2+}]_e$-dependent depression of the SLC41A1-related efflux as the underlying mechanism. Nevertheless, the $[Mg^{2+}]_i$ increase levels off at about 1 mmol liter^{-1}, far below the electrochemical equilibrium for Mg^{2+} under our experimental conditions. This could be attributable to a negative feedback regulation of TRPM7-mediated Mg^{2+} transport or the existence of another unknown Mg^{2+} efflux mechanism, such as the Na^+/Mg^{2+} exchanger in HEK293 cells (10).

At a functional level, a DIDS-sensitive anion-linked Mg^{2+} efflux system has been described in ventricular heart muscle cells (8). Interestingly, abundant levels of the SLC41A1 transcript has been found in the heart (14) and, together with our data, this makes the protein a good candidate for being the proposed efflux pathway. The failure of H_2-DIDS to change $[Mg^{2+}]_i$ in our study does not exclude this possibility because it could result from complete inhibition of SLC41A1-related Mg^{2+} transport by the unphysiologically high extracellular $[Mg^{2+}]$ of 10 mmol liter^{-1} used in our experiments. Low affinity (K_m for $[Mg^{2+}]_e$ about 2 to 6 mmol liter^{-1}), slow and anion-linked (mostly HCO_3^- and Cl^-) Mg^{2+} transporters also have been functionally described in the basolateral membrane of enterocytes (40, 41), erythrocytes (42), and ruminal epithelial cells (43).

In some studies (42), Na^+-independent Mg^{2+} efflux was accompanied by channel-mediated and, therefore, separate Cl^- efflux. This corresponds to our data showing that SLC41A1-related DIDS-blockable Cl^- conductance and $[Mg^{2+}]_i$ changes in +tet HEK293-(SLC41A1) cells are not directly linked. Rather, as described in other studies, endogenous Cl^- channels are activated simply by the reduction of intracellular Mg^{2+}, a condition that would also favor Mg^{2+} transport by TRPM7. An investigation of the functional role of the observed Cl^- conductance was beyond the scope of this study. However, the free intracellular $[Mg^{2+}]$ is known to be an important regulator of various ion channels, *e.g.* K^+ and Na^+ channels, with very different functions depending on the cell type. Activation of SLC41A1-related Mg^{2+} efflux by at present unknown mechanisms can thus play a special role in such processes.

CoHex is the only known Mg^{2+} channel inhibitor showing significant blocking effects on Mg^{2+} transport conducted by the bacterial CorA and the mitochondrial Mrs2 channels (13, 35, 44). Here, we demonstrate that CoHex significantly (approximately 50%) and reversibly inhibits the Mg^{2+} conductance of the TRPM7 ion channels while leaving SLC41A1-mediated $[Mg^{2+}]_i$ change unaffected. Hence, CoHex may prove to interfere with channel-based Mg^{2+} transport mechanisms but not carrier-based mechanisms, increasing the possibilities of identifying distinct Mg^{2+} transport mechanisms in various cell systems. Moreover these results give some indication that SLCA1 functions as an Mg^{2+} carrier rather than as a channel. An additional feature functionally pointing to a carrier mechanism is the temperature sensitivity of the SLCA1-related Mg^{2+} change. Wolf *et al.* (45) have found a similar 80% reduction of Na^+/Mg^{2+} exchanger activity after a temperature reduction from 37 to 15–18 °C, although the same temperature change has no significant effect on Mg^{2+} uptake by the mitochondrial Mg^{2+} channel Mrs2 (13).

Goytain and Quamme (15) observed Mg^{2+} currents after overexpression of mouse SLC41A1 in *Xenopus* oocytes. This, in contrast to our data, points to a channel-like behavior of mouse SLC41A1. Some possible explanation for these diverse results should be given here. One explanation is the simple assumption that, during evolution, the hSLC41A1 Mg^{2+} carrier evolved from the mouse SLC41A1 ion channel. SLC41A1 from mouse and human are sequentially almost identical (92% identity and 92% similarity, BlastP version 2.2.9; mSLC41A1 protein sequence Q8BJA3/NCBI was blasted against hSLC41A1 protein sequence NP776253/NCBI); thus, on the basis of "structures predetermine functions," they could transport Mg^{2+} in a similar manner. However, this assumption can be easily refuted by considering that certain point mutation(s) can alter not only

the ion specificity of the transporter(s) but also the mechanism(s) of the ion transport itself (46–48).

Another explanation for the above mentioned difference might be that interactions between SLC41A1 and its binding partners keep the protein functioning as a Mg^{2+} carrier in mammalian cells, whereas when it is overexpressed in *Xenopus* oocytes, *Salmonella*, or any other non-mammalian expression system, the quantitative and/or qualitative lack of such binding partners result in SLC41A1 functioning as an ion channel. This hypothesis is also supported by the finding that Mg^{2+} accumulation observed after the overexpression of *hSLC41A1* in *Salmonella* occurs rapidly and resembles the kinetics of Mg^{2+} transport conducted via the CorA channel (27).[8] Although we favor this explanation over the first, further experimental investigation will be necessary to describe its molecular basis. In conclusion, our results show that hSLC41A1 represents a functionally active Mg^{2+} carrier mediating Mg^{2+} efflux in mammalian cell systems.

Acknowledgments—We are grateful to Reinhold Penner (The Queen's Medical Center), Rudolf J. Schweyen (Max F. Perutz Laboratories), and Jean-Pierre Kinet (Beth Israel Deaconess Medical Center, Boston, MA) for helpful criticism, to Hans-Christian Aasheim (Radium Hospital, Oslo, Norway) for sending us the pGEM-T-hSLC41A1, Peter Spindler (ARC Seibersdorf research GmbH, Austria) for assisting us with ICP-MS analyses, and Mahealani Monteilh-Zoller (QMC, Honolulu), Renate Brose (FBN Dummerstorf), and Heike Pröhl (FBN Dummerstorf) for competent technical support. We also thank Dr. Theresa Jones for linguistic corrections.

REFERENCES

1. Cowan, J. A. (2002) *Biometals* **15,** 225–235
2. Hartwig, A. (2001) *Mutat. Res.* **475,** 113–121
3. Bara, M., and Guiet-Bara, A. (2001) *Magn. Res.* **14,** 11–18
4. Kisters, K., Tokmak, F., Kosch, M., Dietl, K. H., and Westermann, G. (1999) *Int. J. Angiol.* **8,** 154–156
5. Saris, N. E., Mervaala, E., Karppanen, H., Khawaja, J. A., and Lewenstam, A. (2000) *Clin. Chim. Acta* **294,** 1–26
6. Barbagallo, M., Dominguez, L. J., Brucato, V., Galioto, A., Pineo, A., Ferlisi, A., Tranchino, E., Belvedere, M., Putignano, E., and Costanza, G. (2007) in *New Perspectives in Magnesium Research* (Nishizawa, Y., Morii, H., and Durlach, J., eds) pp. 213–23, Springer-Verlag, London
7. Quamme, G. A., and Rabkin, S. W. (1990) *Biochem. Biophys. Res. Commun.* **167,** 1406–1412
8. Ödblom, M. P., and Handy, R. D. (1999) *Biochem. Biophys. Res. Commun.* **264,** 334–337
9. Schweigel, M., Vormann, J., and Martens, H. (2000) *Am. J. Physiol.* **278,** G400–G408
10. Schweigel, M., Park, H. S., Etschmann, B., and Martens, H. (2006) *Am. J. Physiol.* **290,** G56–G65
11. Chubanov, V., Gudermann, T., and Schlingmann, K. P. (2005) *Pflugers Arch.* **451,** 228–234
12. Schmitz, C., Perraud, A. L., Johnson, C. O., Inabe, K., Smith, M. K., Penner, R., Kurosaki, T., Fleig, A., and Scharenberg, A. M. (2003) *Cell* **114,** 191–200
13. Kolisek, M., Zsurka, G., Samaj, J., Weghuber, J., Schweyen, R. J., and Schweigel, M. (2003) *EMBO J.* **22,** 1235–1244
14. Wabakken, T., Rian, E., Kveine, M., and Aasheim, H. C. (2003) *Biochem. Biophys. Res. Commun.* **306,** 718–724
15. Goytain, A., and Quamme, G. A. (2005) *Physiol. Genomics* **21,** 337–342
16. Goytain, A., and Quamme, G. A. (2005) *Biochem. Biophys. Res. Commun.* **330,** 701–705
17. Sahni, J., Nelson, B., and Scharenberg, A. M. (2006) *Biochem. J.* **401,** 505–513
18. Wang, C. Y., Shi, J. D., Yang, P., Kumar, P. G., Li, Q. Z., Run, Q. S., Su, Y. C., Scott, H. S., Kao, K. J., and She, J. X. (2004) *Gene* (*Amst.*) **306,** 37–44
19. Goytain, A., and Quamme, G. A. (2005) *Physiol. Genomics* **22,** 382–389
20. Goytain, A., and Quamme, G. A. (2005) *BMC Genomics* **6,** 48
21. Goytain, A., Hines, R., El-Husseini, A., and Quamme, G. A. (2007) *J. Biol. Chem.* **282,** 8060–8068
22. Hediger, M. A., Romero, M. F., Peng, J. B., Rolfs, A., Takanaga, H., and Bruford, E. A. (2004) *Pflügers Arch. Eur. J. Physiol.* **447,** 465–468
23. Towsend, D. E., Esenwine, A. J., George, J., 3rd, Bross, D., Maguire, M. E., and Smith, R. L. (1995) *J. Bacteriol.* **177,** 5350–5354
24. Smith, R. L., Thompson, L. J., and Maguire, M. E. (1995) *J. Bacteriol.* **177,** 1233–1238
25. Bullas, L. R., and Ryu, J. I. (1983) *J. Bacteriol.* **156,** 471–474
26. Nelson, D. L., and Kennedy, E. P. (1971) *J. Biol. Chem.* **246,** 3042–3049
27. Froschauer, E. M., Kolisek, M., Dietrich, F., Schweigel, M., and Schweyen, R. J. (2004) *FEMS Microbiol. Lett.* **237,** 49–55
28. Swamy, M., Siegers, G. M., Minguet, S., Wollscheid, B., and Schamel, W. A. (2006) *Sci. STKE* **345,** l4
29. Grynkiewicz, G., Poenie, M., and Tsien, R. Y. (1985) *J. Biol. Chem.* **260,** 3440–3450
30. Jin, L., Amaya-Mazo, X., Apel, M. E., Sankisa, S. S., Johnson, E., Zbyszynska, M. A., and Han, A. (2007) *Biophys. Chem.* **128,** 185–196
31. Urbanowski, J. L., and Piper, R. C. (1999) *J. Biol. Chem.* **274,** 38061–38070
32. Chubanov, V., Waldegger, S., Mederos y Schnitzler, M., Vitzthum, H., Sassen, M. C., Seyberth, H. W., Konrad, M., and Gudermann, T. (2004) *Proc. Natl. Acad. Sci. U. S. A.* **101,** 2894–2899
33. Reddy, M. M., and Quinton, P. M. (1994) *J. Membr. Biol.* **140,** 57–67
34. Meyer, K., and Korbmacher, C. (1996) *J. Gen. Physiol.* **108,** 177–193
35. Kucharski, L. M., Lubbe, W. J., and Maguire, M. E. (2000) *J. Biol. Chem.* **275,** 16767–16773
36. Nadler, M. J., Hermosura, M. C., Inabe, K., Perraud, A. L., Zhu, Q., Stokes, A. J., Kurosaki, T., Kinet, J. P., Penner, R., Scharenberg, A. M., and Fleig, A. (2001) *Nature* **41,** 590–595
37. Hmiel, S. P., Snavely, M. D., Florer, J. B., Maguire, M. E., and Miller, C. G. (1989) *J. Bacteriol.* **171,** 4742–4751
38. Smith, R. L., Gottlieb, E., Kucharski, L. M., and Maguire, M. E. (1998) *J. Bacteriol.* **180,** 2788–2791
39. He, Y., Yao, G., Savoia, G., and Touyz, R. M. (2005) *Circ. Res.* **96,** 207–215
40. Bijvelds, M. J., Kolar, Z. I., Wendelaar Bonga, S. E., and Flik, G. (1996) *J. Membr. Biol.* **154,** 217–225
41. Jüttner, R., and Ebel, H. (1999) *Biochim. Biophys. Acta* **1370,** 51–63
42. Günther, T., and Vormann, J. (1995) *Biochim. Biophys. Acta* **1234,** 105–110
43. Schweigel, M., and Martens, H. (2003) *Am. J. Physiol.* **285,** G45–G53
44. Snavely, M. D., Florer, J. B., Miller, C. G., and Maguire, M. E. (1989) *J. Bacteriol.* **171,** 4761–4766
45. Wolf, F. I., Di Francesco, A., Covacci, V., and Cittadani, A. (1997) in *Advances in Magnesium Research* (Smetana, R., ed) Suppl. 1, pp. 490–496, John Libbey and Co., Ltd, London
46. Gunthorpe, M. J., and Lummis, S. C. (2001) *J. Biol. Chem.* **276,** 10977–10983
47. Gadsby, D. C. (2004) *Nature* **427,** 795–797
48. Scheel, O., Ydebik, A. A., Lourdel, S., and Jentsch, T. J. (2005) *Nature* **436,** 424–427

[8] G. Sponder and M. Kolisek, manuscript in preparation.